




**Benchmarks of generalized hydrodynamics for one-dimensional Bose gases**R. S. Watson , S. A. Simmons , and K. V. Kheruntsyan *School of Mathematics and Physics, University of Queensland, Brisbane, Queensland 4072, Australia* (Received 12 August 2022; revised 23 February 2023; accepted 14 April 2023; published 5 May 2023)

Generalized hydrodynamics (GHD) is a recent theoretical approach that is becoming a go-to tool for characterizing out-of-equilibrium phenomena in integrable and near-integrable quantum many-body systems. Here, we benchmark its performance against an array of alternative theoretical methods, for an interacting one-dimensional Bose gas described by the Lieb-Liniger model. In particular, we study various quantum shock wave scenarios, along with a quantum Newton’s cradle setup, for various interaction strengths and initial temperatures. We find that GHD generally performs very well at sufficiently high temperatures or strong interactions. For low temperatures and weak interactions, we highlight situations where GHD, while not capturing interference phenomena on short lengthscales, can describe a coarse-grained behavior based on convolution averaging that mimics finite imaging resolution in ultracold atom experiments. In a quantum Newton’s cradle setup based on a double-well to a single-well trap quench, we find that GHD with diffusive corrections demonstrates excellent agreement with the predictions of a classical field approach.

DOI: [10.1103/PhysRevResearch.5.L022024](https://doi.org/10.1103/PhysRevResearch.5.L022024)

*Introduction.* The study of dynamics of integrable and near-integrable quantum many-body systems has been a thriving area of research for more than a decade since the landmark experiments on relaxation in the quantum Newton’s cradle setup [1] and in coherently split one-dimensional (1D) Bose gases [2]. During this time, an in-depth understanding of the mechanisms of thermalization and emergent out-of-equilibrium phenomena within these systems has been developed [3–8]. A recent breakthrough in this area has been the discovery of the theory of generalized hydrodynamics (GHD) [9,10] (for recent reviews, see Refs. [11–13]). This new theory is capable of simulating large-scale dynamics of integrable and near-integrable systems across a range of particle numbers and interaction strengths significantly broader than those accessible using previous approaches [14–16]. Because of its broad applicability, GHD is currently regarded as well on its way to becoming “a standard tool in the description of strongly interacting 1D quantum dynamics close to integrable points” [16].

In the years since its discovery, GHD has been rapidly developed to include diffusive terms [17–22], particle loss [23], calculations of quantum and Euler-scale correlations [24–29], and the incorporation of numerous beyond-Euler scale effects [30–33] (see also Refs. [34–37] in a special issue). Recently, GHD applied to a 1D Bose gas has been experimentally verified in a variant of the quantum Newton’s cradle setup in the weakly interacting regime [15] and in a harmonic trap quench in the strongly interacting regime [16]. In both cases, GHD provided an accurate coarse-grained

model of the dynamics, exceeding conventional (classical) hydrodynamics. In addition to comparisons with experiments, GHD was benchmarked against other established theoretical approaches—most prominently for the 1D Bose gas and the XXZ spin chain [9,10,14,15,24,27,33,38–43]. As the purpose of these initial benchmarks was to validate GHD, the typical dynamical scenarios considered were in regimes where GHD was expected to be a valid theory. In all such cases GHD demonstrated very good agreement with the alternative approaches. On the other hand, in scenarios involving, for example, short wavelength density oscillations due to interference phenomena (which are not captured by GHD), it was conjectured that GHD would nevertheless adequately describe spatial coarse-grained averages of the more accurate theories [14,15,32]. More generally, it is of significant interest to scrutinize the performance of GHD by extending its benchmarks to a more challenging set of dynamical scenarios. This is important for understanding exactly how GHD breaks down when it is pushed towards and beyond the limits of its applicability.

In this Letter, we systematically benchmark the performance of GHD for the 1D Bose gas in several paradigmatic out-of-equilibrium scenarios. In particular, we focus on the regime of dispersive quantum shock waves emanating from a localized density bump of the type explored recently in Ref. [44]. We use an array of theoretical approaches, including finite temperature  $c$ -field methods, the truncated Wigner approximation, and the numerically exact infinite matrix product state (iMPS) method, spanning the entire range of interaction strengths, from the nearly ideal Bose gas to the strongly interacting Tonks-Girardeau (TG) regime. We also analyze the dynamics of a localized density dip which sheds gray solitons, hence benchmarking GHD in scenarios not previously considered. In doing so, we address the question of how well GHD predictions agree with coarse-grained averaging of the results

---

*Published by the American Physical Society under the terms of the Creative Commons Attribution 4.0 International license. Further distribution of this work must maintain attribution to the author(s) and the published article’s title, journal citation, and DOI.*

of the more accurate theoretical approaches. Additionally, we explore the dynamics of a thermal quasicondensate in a quantum Newton's cradle setup [15,45,46] using Navier-Stokes type diffusive GHD [17,20,47], and we address the question of characteristic thermalization rates [19,45].

*Expansion from a localized density bump.* We begin our analysis by considering dispersive quantum shock waves of the type studied recently in Ref. [44]. More specifically, we first focus on the weakly interacting regime of the 1D Bose gas of  $N$  particles described by the Lieb-Liniger model [48,49], and we consider the dynamics of the oscillatory shock wave train generated through a trap quench from an initially localized perturbation on top of a flat background to free propagation in a uniform box of length  $L$  with periodic boundary conditions [50,51]. The weakly interacting regime is characterized by the Lieb-Liniger dimensionless interaction parameter  $\gamma_{\text{bg}} = mg/\hbar^2 \rho_{\text{bg}} \ll 1$  [48,52], defined with respect to the background particle number density  $\rho_{\text{bg}}$ , where  $g > 0$  is the strength of repulsive contact interaction and  $m$  is the mass of the particles.

In our first example, we consider the case of a large total number of particles,  $N = 2000$ , and  $\gamma_{\text{bg}} = 0.01$ , so that the gas is in the Thomas-Fermi regime where the interaction energy per particle dominates the kinetic energy. We assume that the gas is initialized in the zero-temperature ( $T = 0$ ) ground state of a dimple trap that results in the density profile of Eq. (A1) given in Appendix A. At time  $\tau = 0$ , the dimple trap is suddenly switched off, and we follow the evolution of the system in a uniform 1D trap. In Figs. 1(a) and 1(b), we show snapshots of the density profiles at different times and compare the GHD results with those obtained using the mean field Gross-Pitaevskii equation (GPE) and the truncated Wigner approximation (TWA) which incorporates the effect of quantum fluctuations ignored in the GPE [53]. The snapshot at  $\tau = 0.00014$ , which corresponds to the onset of a shock formation due to a large density gradient, shows excellent agreement between GHD and the more accurate microscopic approaches. Such an agreement at early times is remarkable given that GHD, which is derived here at Euler scale [54], becomes formally exact only in the limit of infinitely large lengthscales and timescales [11,14,27].

Past this time, the GPE and TWA show the formation of an oscillatory shock wave train, which has been identified in Ref. [44] as a result of self-interference of the expanding density bump with its own background. The interference contrast in this regime is generally large, even though the quantum fluctuations present in the TWA approach cause a visible reduction in contrast compared with the mean-field GPE result. The GHD prediction, on the other hand, completely fails to capture the oscillations, as these occur on a microscopic lengthscale. The characteristic period of oscillations here (which we note are chirped) is given approximately by the healing length  $l_h = \hbar/\sqrt{mg\rho_{\text{bg}}}$  ( $l_h/L = 0.0057$ ), which is smaller than the width  $\sigma$  ( $\sigma/L = 0.02$ ) of the initial bump and hence represents the shortest lengthscale of the problem in the bulk of the shock wave train. Thus, even though the local density approximation (required for GHD to be applicable to an inhomogeneous system in the first place) is valid for the initial Thomas-Fermi density profile, the failure of GHD at later times is expected since it is not supposed to capture

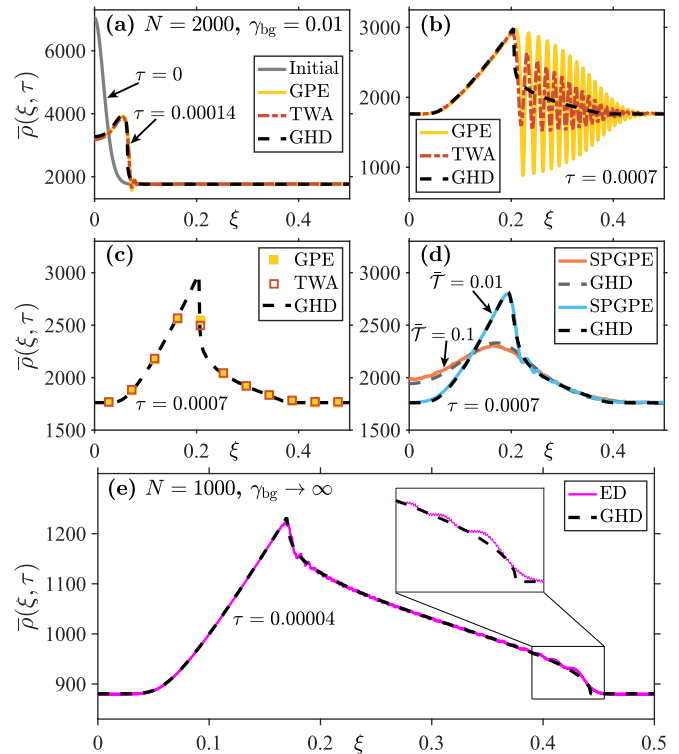


FIG. 1. Dimensionless density profiles  $\bar{\rho} = \rho L$  of quantum shock waves in the 1D Bose gas, as a function of the dimensionless coordinate  $\xi \equiv x/L$  at different times  $\tau \equiv \hbar t/mL^2$ . In panel (a) we show the initial ( $\tau = 0$ ) and time-evolved ( $\tau = 0.00014$ ) profiles of a weakly interacting gas at zero temperature, for  $\gamma_{\text{bg}} = 0.01$  and  $N = 2000$  (with  $N_{\text{bg}} \simeq 1761$  being the number of particles in the background). Due to the symmetry about the origin, we only show the densities for  $\xi > 0$ . In panel (b), the time-evolved profile is shown at  $\tau = 0.0007$ . Panel (c) demonstrates the results of finite resolution averaging of both GPE and TWA data from panel (b) and compares them with the same GHD result. Panel (d) shows the same system as in panel (b), but at finite temperatures, simulated using the stochastic-projected GPE (SPGPE) [44]; the dimensionless temperature  $\bar{T}$  here is defined according to  $\bar{T} = T/T_d$ , where  $T_d = \hbar^2 \rho_{\text{bg}}^2 / 2mk_B$  [52]. Panel (e) compares GHD predictions with exact diagonalization (ED) results in the TG regime ( $\gamma_{\text{bg}} \rightarrow \infty$ ) for  $N = 1000$  ( $N_{\text{bg}} \simeq 884$ ), at  $\tau = 0.00004$ . In all examples, the initial profiles are characterized by the amplitude height  $\beta = 1$  and the dimensionless width of the bump  $\bar{\sigma} = 0.02$ ; see Appendix A for details.

phenomena on microscopic lengthscales, which emerge here dynamically.

Despite this failure, GHD clearly captures the average density of the oscillations for the fully formed shock wave train, similar to that shown in Ref. [13]. This is consistent with the analysis of Bettelheim [55], who showed that the Whitham approach, which allows one to write equations for averaged quantities in the oscillatory shock wave train, is equivalent to GHD in the semiclassical limit ( $c = mg/\hbar^2 \rightarrow 0$ ) of the Lieb-Liniger model [56,57]. This is also consistent with the expectation that GHD in an interfering region would correspond to a coarse-grained average density [14,15]. To quantitatively assess this expectation, we perform a type of convolution averaging that mimics the finite resolution of

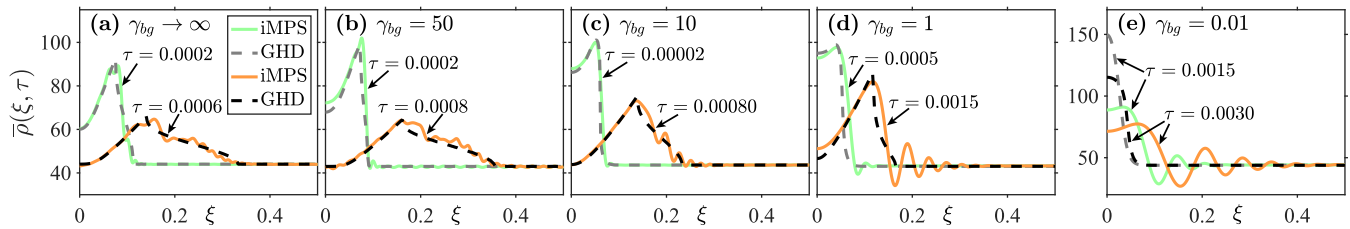


FIG. 2. Quantum shock waves at zero temperature for  $N = 50$  particles ( $N_{bg} \simeq 44.03$ ), over the entire range of interaction strengths. In all examples, the initial density profiles (not shown) closely match Eq. (A1) in Appendix A, with  $\beta = 1$  and  $\bar{\sigma} = 0.02$ . In all panels, we show the GHD (dashed lines) and iMPS (solid lines) results for the evolved density profiles at two time instances. In panel (a) there is no phase coherence beyond the mean interparticle separation ( $1/\rho_{bg}L \simeq 0.0227$ ), whereas in panel (e) the shortest lengthscale that determines the characteristic period of oscillations is given by the width of the initial Gaussian bump  $\sigma$  ( $\sigma/L = 0.02$ ), which is much smaller than the healing length  $l_h$  ( $l_h/L = 0.227$ ).

*in situ* imaging systems used in quantum gas experiments (see Appendix B). As the imaging resolution is usually unable to resolve wavelengths on the order of the healing length (typically in the submicron range), one expects that such averaging will smear out the interference fringes seen in the GPE and TWA data—just as GHD implicitly does. In Fig. 1(c) we show the results of convolution-averaged density profiles performed on the GPE and TWA data of Fig. 1(b) and compare them with the same GHD curve. The level of agreement between all three curves is now remarkable—a result which was not *a priori* obvious for both GPE and TWA under this model of coarse-graining. This highlights the quantitative success of GHD in describing the dynamics on a large scale despite interference or short-wavelength phenomena being present.

In our second set of examples, shown in Fig. 1(d), we consider the same shock wave scenario, except now for a phase-fluctuating quasicondensate at finite temperatures. Here, the effect of thermal fluctuations is expected to lead to a smearing of the interference contrast due to a reduced thermal phase coherence length in the system,  $l_T = \hbar^2 \rho_{bg} / m k_B T$  [58–60]. A well-established theoretical approach to model this is a  $c$ -field stochastic-projected GPE (SPGPE) approach [61,62] (see also Refs. [45,63–65]), and we indeed observe such smearing in Fig. 1(d) [66], in addition to seeing the expected very good agreement of GHD with these  $c$ -field results.

Our third example is shown in Fig. 1(e) and lies in the TG regime of infinitely strong interactions,  $\gamma_{bg} \rightarrow \infty$ . It further illustrates the same observation—that the performance of GHD improves with the loss of phase coherence in the system, wherein interference phenomena are suppressed. Here, we compare the predictions of GHD for the shock wave scenario at  $T = 0$  with the results of exact diagonalization. In the TG regime, the system does not possess phase coherence beyond the mean interparticle separation  $1/\rho_{bg}$ , hence the absence of interference fringes in the evolution of a density bump whose initial width is larger than  $1/\rho_{bg}$  [44]. Accordingly, we see very good agreement of GHD with exact diagonalization, ignoring the small-amplitude density ripples that can be seen in the exact result. Such density ripples (which we note have an origin different than that of Friedel oscillations) have been predicted to occur in the ideal Fermi gas by Bettelheim and Glazman [67] (see also Ref. [68]). By the Fermi-Bose mapping [69,70], these same ripples should emerge in the TG gas, which we confirm here through exact diagonalization.

However, their description lies beyond the scope of GHD as a large-scale theory [71].

The final set of examples for the evolution of a density bump is shown in Fig. 2. Here, we consider a range of interaction strengths, starting from very strong and going back [from Figs. 2(a) to 2(e)] to weak interactions, all at zero temperature and  $N = 50$ . We compare the GHD results with iMPS simulations, which are numerically exact at all interaction strengths [44]. At this relatively low particle number, the strongly interacting regime displays Friedel oscillations which appear in the iMPS result and are, as expected, absent from the prediction of GHD. However, there is generally good agreement between GHD and iMPS at large scale. As the interaction strength is reduced, and hence the phase coherence of the gas increases, the Friedel oscillations disappear and interference fringes return, which now have period  $\sim \sigma$  (with  $\sigma < l_h$ ) since the gas is no longer in the Thomas-Fermi regime. The worst performance of GHD is observed for  $\gamma_{bg} = 0.01$ , which lies in the nearly ideal (noninteracting) Bose gas regime for  $N = 50$ . In this regime, the local density approximation, intrinsic to GHD [14–16,52], is no longer valid even for the initial density profile, and we see that Euler-scale GHD breaks down both spatially and temporally, explaining the failure of GHD to agree with iMPS results even in the coarse-grained sense.

In addition to considering the dynamics of a localized density bump, we have also analyzed the evolution of an initial density dip in a uniform background. This scenario is known to shed a train of gray solitons in the mean-field GPE treatment [50,51,72], and the results of the comparison of GHD simulations with those of GPE and TWA are presented in Appendix C. The overall conclusions regarding the performance of GHD in this scenario are similar to those for a density bump, including good agreement of GHD with coarse-grained averages of GPE and TWA results in the soliton train region.

*Quantum Newton's cradle in a thermal quasicondensate.* Our final scenario for benchmarking GHD is in a variant of the quantum Newton's cradle setup for a weakly interacting 1D Bose gas in the quasicondensate regime. Namely, we analyze the release from a symmetric double-well trap to a single-well harmonic trap of frequency  $\omega$ , similar to the type utilized in Ref. [15]. Here, we use the SPGPE to simulate collisional dynamics and eventual thermalization, as in Ref. [45], and for the sake of one-to-one comparison, we also simulate the same system using the Navier-Stokes type of diffusive GHD

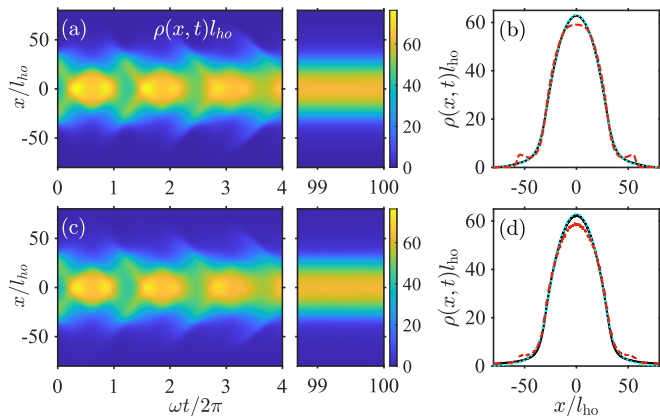


FIG. 3. Evolution and thermalization of the density distribution  $\rho(x, t)$  in a quantum Newton's cradle setup initialized from a double-well to a single-well trap quench, simulated using Navier-Stokes GHD [panels (a) and (b)] and SPGPE [panels (c) and (d)]. The initial cloud of  $N = 3340$  atoms at temperature  $\tilde{T} = 205$  (in harmonic oscillator units) is prepared in a thermal equilibrium state of a symmetric double-well trap potential (see Appendix D for details). Panel (b) demonstrates the relaxed density profile of the Navier-Stokes GHD evolution at  $t = 100/(\omega/2\pi)$  (black solid line), alongside a best-fit thermal equilibrium profile from Yang-Yang thermodynamics at  $\tilde{T} \simeq 213$  (cyan dotted line), and an additional GHD density profile at earlier time  $t = 6.79/(\omega/2\pi)$  (red dashed line). Panel (d) is the same as panel (b), but for the SPGPE, with the relaxed density profile at  $t \simeq 100/(\omega/2\pi)$ , a Yang-Yang thermodynamic density profile of  $\tilde{T} \simeq 216$ , and an additional density profile at  $t = 6.81/(\omega/2\pi)$ .

[17,47], solved using a second-order backwards-implicit algorithm [18,39,73].

Comparison of the results using the two methods are shown in Fig. 3, where we illustrate the evolution of the density distribution [panel (a) for diffusive GHD, and panel (c) for SPGPE] over the initial few oscillations, as well as after a sufficiently long time, when the system has already thermalized. In Ref. [74] we give further details of how the final relaxed states were assessed within GHD and the SPGPE, whereas here, in Figs. 3(b) and 3(d), we simply show the respective relaxed density profiles, along with their corresponding thermal equilibrium profiles from Yang-Yang thermodynamics [52,74–78], as well as density profiles at earlier times illustrating their contrast to the relaxed state. The overall conclusion here is that GHD demonstrates excellent agreement with SPGPE in both short- and long-term dynamics, as well as in the characteristic thermalization rate [79].

We have also simulated the quantum Newton's cradle experiment in the original Bragg pulse scenario [1], except in a weakly interacting quasicondensate regime. In this scenario, we observe different thermalization rates in GHD and SPGPE simulations, and we discuss these results and the reasons behind the discrepancy in the Supplementary Material [74].

*Summary.* We have benchmarked GHD in a variety of out-of-equilibrium scenarios in a 1D Bose gas against alternative theoretical approaches which are not limited to long-wavelength excitations. In particular, we have focused on systems supporting dispersive quantum shock waves and soliton trains, demonstrating that GHD generally agrees with the

predictions of these approaches at sufficiently high temperatures and strong interactions. Here, the good agreement stems from a reduced phase coherence length of the gas, which in turn leads to a suppression of interference phenomena and therefore an absence of high-contrast short-wavelength interference fringes in the density. At low temperatures and weak interactions, where interference phenomena are more pronounced, the predictions of GHD only agree with a coarse-grained convolution averaging approximation. The effect of such averaging is similar to having finite imaging resolution in quantum gas experiments and explains why GHD may perform well when compared to experiments, whilst departing from the predictions of theoretical approaches that are valid at short wavelengths. We have also benchmarked Navier-Stokes GHD within a quantum Newton's cradle setup for a double-well to a single-well trap quench of a weakly interacting quasicondensate, observing excellent agreement with the SPGPE in both the transient dynamics and the final relaxed state, as well as in the characteristic relaxation timescale.

*Acknowledgments.* K.V.K. acknowledges stimulating discussions with I. Bouchoule, M. J. Davis, and D. M. Gangardt. This work was supported through the Australian Research Council (ARC) Discovery Project under Grant No. DP190101515.

#### APPENDIX A: PARAMETRIZATION OF THE DENSITY BUMP

The initial density profile in Fig. 1(a), in dimensionless units, is set to

$$\bar{\rho}(\xi, \tau = 0) = \bar{\rho}_{\text{bg}}(1 + \beta e^{-\xi^2/2\bar{\sigma}^2})^2, \quad (\text{A1})$$

where the dimensionless coordinate, time, and density are introduced, respectively, according to  $\xi \equiv x/L$ ,  $\tau \equiv \hbar t/mL^2$ , and  $\bar{\rho}(\xi, \tau) \equiv \rho(x, t)L$ , with  $\bar{\rho}_{\text{bg}} = \rho_{\text{bg}}L = N_{\text{bg}}$  being the dimensionless background density equivalent to the total number of particles in the background,  $N_{\text{bg}} = N/\{1 + \frac{\sqrt{\pi}\beta\sigma}{L}[\beta \text{erf}(\frac{L}{2\sigma}) + 2\sqrt{2} \text{erf}(\frac{L}{2\sqrt{2}\sigma})]\}$  from the normalization. In addition, the width and the amplitude of the bump above the background are characterized by the dimensionless parameters  $\bar{\sigma} \equiv \sigma/L$  and  $\beta > 0$ , respectively.

The associated trapping potential that is required for the preparation of such a density profile as an initial ground or thermal equilibrium state of the 1D Bose gas in different regimes is discussed in Ref. [44]. Within the mean-field approximation, described by the Gross-Pitaevskii equation, the density profile of Eq. (A1) corresponds to the mean-field amplitude being initialized as a simple Gaussian bump superimposed on a constant background,  $\bar{\Psi}(\xi, \tau = 0) = \bar{\Psi}_{\text{bg}}(1 + \beta e^{-\xi^2/2\bar{\sigma}^2})$ , with  $\bar{\rho}_{\text{bg}} = |\bar{\Psi}_{\text{bg}}|^2$ .

#### APPENDIX B: FINITE RESOLUTION AVERAGING

The finite resolution averaging procedure implemented in Fig. 1(c) emulates the finite spatial resolution of experimental absorption imaging systems. Following Ref. [80], we denote the impulse response function of the imaging system by  $\mathcal{A}(x)$ ,

which we here assume to be a normalized Gaussian. The impulse response for a pixel of width  $\Delta$  centered at  $x_p$  is then

$$\mathcal{F}(x) = \int_{x_p - \Delta/2}^{x_p + \Delta/2} dx' \mathcal{A}(x' - x). \quad (\text{B1})$$

The *measured* atom number in the given pixel is then given by

$$N_m = \mathcal{N} \int_{-\infty}^{+\infty} dx \mathcal{F}(x) \rho(x), \quad (\text{B2})$$

where  $\mathcal{N}$  provides the correct normalization for the total particle number in the limit of zero pixel width.

In our particular example of such averaging, the density profile  $\rho(x)$  (at any given time step, with the time argument  $t$  being omitted here for notational simplicity) is convoluted with a Gaussian resolution function of width  $w = 1 \mu\text{m}$  and then averaged over a finite pixel size  $\Delta = 4.5 \mu\text{m}$ , as in Ref. [80]. These absolute values translate to dimensionless values of  $w/L = 0.01$  and  $\Delta/L = 0.045$ , assuming  $L \sim 100 \mu\text{m}$ , with results being generally insensitive to the exact values of these parameters around these typical values. For comparison, the healing length in this example is equal to  $l_h/L = 0.0057$ . Considering  $^{87}\text{Rb}$  atoms, which have a scattering length of  $a \simeq 5.3 \text{ nm}$ , in a system of size  $L = 100 \mu\text{m}$ , this corresponds to an absolute healing length of  $l_h = 0.57 \mu\text{m}$ . These choices of dimensionless parameters, and  $\gamma_{\text{bg}} = 0.01$ , can be realized at a background density of  $\rho_{\text{bg}} \simeq 1.8 \times 10^7 \text{ m}^{-3}$ , with an interaction parameter  $g \simeq 2\hbar\omega_{\perp}a \simeq 1.4 \times 10^{-38} \text{ J m}$  [81], where  $\omega_{\perp}/2\pi \simeq 1.9 \text{ kHz}$  is the frequency of the transverse harmonic trapping potential.

### APPENDIX C: DYNAMICS OF A LOCALIZED DENSITY DIP

In this Appendix, we present the results of the evolution of a localized density depression, after quenching (at time  $\tau = 0$ ) the initial trap potential with a localized barrier to uniform. We assume that the initial density profile is given by the same Eq. (A1), except with  $\beta$  being negative and satisfying  $-1 < \beta < 0$ .

In Figs. 4(a) and 4(b), we consider the weakly interacting regime (with  $\gamma_{\text{bg}} = 0.01$ ) and show the results of the GPE, TWA, and GHD simulations, for a gas with  $N = 1688$  atoms and the same  $N_{\text{bg}} \simeq 1761$  as in Fig. 1(a). In this scenario, the steep gradient of the shock front forms as the background fluid flows inward and tries to fill the density depression. As a result, one first observes the emergence of large-amplitude structures, forming multiple density troughs, which then evolve into a train of gray solitons propagating away from the origin [50,51,57,72,82,83]. The differences between the TWA and pure mean-field GPE results, seen in Fig. 4(b), are consistent with previous observations [84–86] that quantum fluctuations lower the mean soliton speed and fill in the soliton core. The GHD result, on the other hand, fails to capture the solitonic structures, whose characteristic width (on the order of the microscopic healing length) lies beyond the intended range of applicability of GHD.

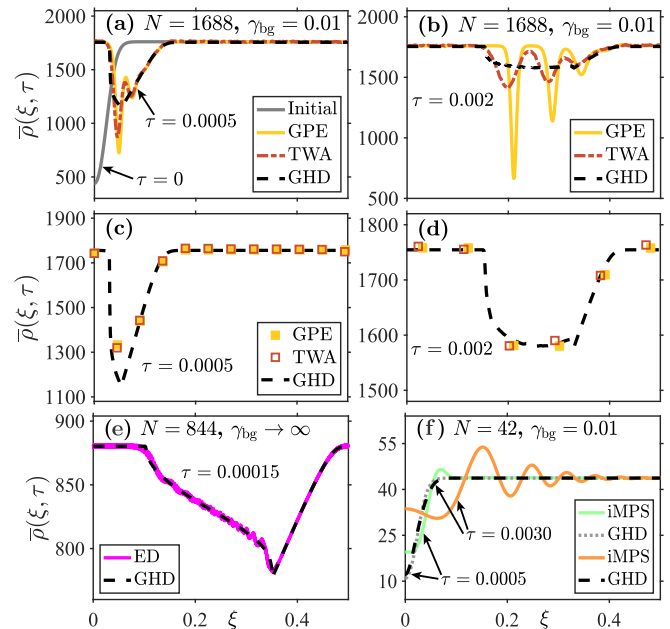


FIG. 4. Evolution of a density dip in a 1D Bose gas. Panel (a) shows the initial ( $\tau = 0$ ) and time-evolved ( $\tau = 0.0005$ ) density profiles from GPE, TWA, and GHD simulations, for  $\gamma_{\text{bg}} = 0.01$  and  $N = 1688$  ( $N_{\text{bg}} \simeq 1761$ ). Panel (b) shows a time-evolved density profile at a later time ( $\tau = 0.002$ ), where we can see a fully formed train of three gray solitons in the mean-field GPE (solid yellow) curve. Panels (c) and (d) compare the same GHD results (notice the different scale of the vertical axis) at  $\tau = 0.0005$  and  $\tau = 0.002$  with the outcomes of finite resolution averaging of both GPE and TWA curves. In panel (e), we show a time-evolved snapshot of the density profile in the TG regime ( $\gamma_{\text{bg}} \rightarrow \infty$ ) for  $N = 844$  ( $N_{\text{bg}} \simeq 880.5$ ), and we compare the GHD result with that of exact diagonalization (ED). Panel (f) is in the nearly ideal Bose gas regime, with  $\gamma_{\text{bg}} = 0.01$  and  $N = 42$  ( $N_{\text{bg}} \simeq 44$ ). In all examples, the initial density profile is given by Eq. (A1) with  $\beta = -0.5$  and  $\bar{\sigma} = 0.02$ .

However, GHD still manages to adequately capture the coarse-grained description of the density across the soliton train, which is rather remarkable. This is seen in Figs. 4(c) and 4(d), where we demonstrate the outcomes of finite resolution averaging applied to the GPE and TWA results of Figs. 4(a) and 4(b), respectively. Similarly to Fig. 1(c), here we used the same normalized Gaussian resolution function of width  $1 \mu\text{m}$  and adopted  $^{87}\text{Rb}$  atoms as an example species for the relevant parameter values (see Appendix B). For Fig. 4(c) we used the same pixel size ( $\Delta = 4.5 \mu\text{m}$ ) as before, whereas for Fig. 4(d), due to the presence of fully formed gray solitons whose width is on the order of  $(2-4)l_h$ , we used a twice larger pixel size ( $\Delta = 9.0 \mu\text{m}$ ). A larger pixel size here results in  $\Delta/l_h \simeq 16 \gg 1$ , which is required in order to comply with the large-scale framework of GHD.

The last two examples, shown in Figs. 4(c) and 4(d), correspond, respectively, to the strongly interacting TG and nearly ideal Bose gas regimes. The overall behavior and conclusions about the performance of GHD in these examples are the same as in the equivalent scenario of the density bump discussed earlier in Figs. 1(e) and 2(a).

#### APPENDIX D: PARAMETRIZATION OF THE DOUBLE-WELL TRAP

The initial (prequench) double-well trap potential is set to  $\tilde{V}(\tilde{x}) \simeq 2.16 \times 10^{-3} \tilde{x}^4 - 5.27 \times 10^{-1} \tilde{x}^2$  in dimensionless form, where  $\tilde{x} = x/l_{\text{ho}}$ ,  $\tilde{V} = V/\hbar\omega$ , and  $l_{\text{ho}} = \sqrt{\hbar/m\omega}$ , where

$\omega$  is the postquench single-well harmonic trap frequency. The initial dimensional temperature of the cloud, in harmonic oscillator units, is set to  $\tilde{T} = T/(\hbar\omega/k_B) \simeq 205$ . In this configuration, the initial density profile for a total of  $N = 3340$  atoms is double peaked, with the dimensionless interaction strength at either of the peaks given by  $\gamma_{\text{max}} \simeq 0.0138$ .

- 
- [1] T. Kinoshita, T. Wenger, and D. S. Weiss, A quantum Newton's cradle, *Nature (London)* **440**, 900 (2006).
- [2] S. Hofferberth, I. Lesanovsky, B. Fischer, T. Schumm, and J. Schmiedmayer, Non-equilibrium coherence dynamics in one-dimensional Bose gases, *Nature (London)* **449**, 324 (2007).
- [3] M. Rigol, V. Dunjko, V. Yurovsky, and M. Olshanii, Relaxation in a Completely Integrable Many-Body Quantum System: An *Ab Initio* Study of the Dynamics of the Highly Excited States of 1D Lattice Hard-Core Bosons, *Phys. Rev. Lett.* **98**, 050405 (2007).
- [4] M. Rigol, V. Dunjko, and M. Olshanii, Thermalization and its mechanism for generic isolated quantum systems, *Nature (London)* **452**, 854 (2008).
- [5] M. A. Cazalilla and M. Rigol, Focus on dynamics and thermalization in isolated quantum many-body systems, *New J. Phys.* **12**, 055006 (2010).
- [6] A. Polkovnikov, K. Sengupta, A. Silva, and M. Vengalattore, Colloquium: Nonequilibrium dynamics of closed interacting quantum systems, *Rev. Mod. Phys.* **83**, 863 (2011).
- [7] C. Gogolin and J. Eisert, Equilibration, thermalisation, and the emergence of statistical mechanics in closed quantum systems, *Rep. Prog. Phys.* **79**, 056001 (2016).
- [8] T. Langen, S. Erne, R. Geiger, B. Rauer, T. Schweigler, M. Kuhnert, W. Rohringer, I. E. Mazets, T. Gasenzer, and J. Schmiedmayer, Experimental observation of a generalized Gibbs ensemble, *Science* **348**, 207 (2015).
- [9] B. Bertini, M. Collura, J. De Nardis, and M. Fagotti, Transport in Out-of-Equilibrium XXZ Chains: Exact Profiles of Charges and Currents, *Phys. Rev. Lett.* **117**, 207201 (2016).
- [10] O. A. Castro-Alvaredo, B. Doyon, and T. Yoshimura, Emergent Hydrodynamics in Integrable Quantum Systems Out of Equilibrium, *Phys. Rev. X* **6**, 041065 (2016).
- [11] B. Doyon, Lecture Notes On Generalised Hydrodynamics, *SciPost Phys. Lect. Notes*, 18 (2020).
- [12] I. Bouchoule and J. Dubail, Generalized hydrodynamics in the one-dimensional Bose gas: Theory and experiments, *J. Stat. Mech.: Theory Exp.* (2022) 014003.
- [13] F. H. Essler, A short introduction to generalized hydrodynamics, *Phys. A (Amsterdam, Neth.)*, 127572 (2022).
- [14] B. Doyon, J. Dubail, R. Konik, and T. Yoshimura, Large-Scale Description of Interacting One-Dimensional Bose Gases: Generalized Hydrodynamics Supersedes Conventional Hydrodynamics, *Phys. Rev. Lett.* **119**, 195301 (2017).
- [15] M. Schemmer, I. Bouchoule, B. Doyon, and J. Dubail, Generalized Hydrodynamics on an Atom Chip, *Phys. Rev. Lett.* **122**, 090601 (2019).
- [16] N. Malvania, Y. Zhang, Y. Le, J. Dubail, M. Rigol, and D. S. Weiss, Generalized hydrodynamics in strongly interacting 1D Bose gases, *Science* **373**, 1129 (2021).
- [17] J. De Nardis, D. Bernard, and B. Doyon, Hydrodynamic Diffusion in Integrable Systems, *Phys. Rev. Lett.* **121**, 160603 (2018).
- [18] S. Gopalakrishnan, D. A. Huse, V. Khemani, and R. Vasseur, Hydrodynamics of operator spreading and quasiparticle diffusion in interacting integrable systems, *Phys. Rev. B* **98**, 220303(R) (2018).
- [19] A. Bastianello, A. De Luca, B. Doyon, and J. De Nardis, Thermalization of a Trapped One-Dimensional Bose Gas via Diffusion, *Phys. Rev. Lett.* **125**, 240604 (2020).
- [20] J. Durnin, A. D. Luca, J. D. Nardis, and B. Doyon, Diffusive hydrodynamics of inhomogeneous Hamiltonians, *J. Phys. A: Math. Theor.* **54**, 494001 (2021).
- [21] A. Bastianello, A. D. Luca, and R. Vasseur, Hydrodynamics of weak integrability breaking, *J. Stat. Mech.: Theory Exp.* (2021) 114003.
- [22] V. B. Bulchandani, S. Gopalakrishnan, and E. Ilievski, Superdiffusion in spin chains, *J. Stat. Mech.: Theory Exp.* (2021) 084001.
- [23] I. Bouchoule, B. Doyon, and J. Dubail, The effect of atom losses on the distribution of rapidities in the one-dimensional Bose gas, *SciPost Phys.* **9**, 044 (2020).
- [24] P. Ruggiero, P. Calabrese, B. Doyon, and J. Dubail, Quantum Generalized Hydrodynamics, *Phys. Rev. Lett.* **124**, 140603 (2020).
- [25] P. Ruggiero, P. Calabrese, B. Doyon, and J. Dubail, Quantum generalized hydrodynamics of the Tonks–Girardeau gas: Density fluctuations and entanglement entropy, *J. Phys. A: Math. Theor.* **55**, 024003 (2022).
- [26] B. Doyon, Exact large-scale correlations in integrable systems out of equilibrium, *SciPost Phys.* **5**, 054 (2018).
- [27] F. S. Møller, G. Perfetto, B. Doyon, and J. Schmiedmayer, Euler-scale dynamical correlations in integrable systems with fluid motion, *SciPost Phys. Core* **3**, 016 (2020).
- [28] J. D. Nardis, B. Doyon, M. Medenjak, and M. Panfil, Correlation functions and transport coefficients in generalised hydrodynamics, *J. Stat. Mech.: Theory Exp.* (2022) 014002.
- [29] V. Alba, B. Bertini, M. Fagotti, L. Piroli, and P. Ruggiero, Generalized-hydrodynamic approach to inhomogeneous quenches: Correlations, entanglement and quantum effects, *J. Stat. Mech.: Theory Exp.* (2021) 114004.
- [30] M. Fagotti, Higher-order generalized hydrodynamics in one dimension: The noninteracting test, *Phys. Rev. B* **96**, 220302(R) (2017).
- [31] M. Panfil and J. Pawełczyk, Linearized regime of the generalized hydrodynamics with diffusion, *SciPost Phys. Core* **1**, 002 (2019).
- [32] F. Møller, C. Li, I. Mazets, H.-P. Stimming, T. Zhou, Z. Zhu, X. Chen, and J. Schmiedmayer, Extension of the Generalized Hydrodynamics to the Dimensional Crossover Regime, *Phys. Rev. Lett.* **126**, 090602 (2021).

- [33] A. Bastianello, J. De Nardis, and A. De Luca, Generalized hydrodynamics with dephasing noise, *Phys. Rev. B* **102**, 161110(R) (2020).
- [34] B. Buča, K. Klobas, and T. Prosen, Rule 54: Exactly solvable model of nonequilibrium statistical mechanics, *J. Stat. Mech.: Theory Exp.* (2021) 074001.
- [35] M. Borsi, B. Pozsgay, and L. Pristiyák, Current operators in integrable models: A review, *J. Stat. Mech.: Theory Exp.* (2021) 094001.
- [36] G. A. El, Soliton gas in integrable dispersive hydrodynamics, *J. Stat. Mech.: Theory Exp.* (2021) 114001.
- [37] A. C. Cubero, T. Yoshimura, and H. Spohn, Form factors and generalized hydrodynamics for integrable systems, *J. Stat. Mech.: Theory Exp.* (2021) 114002.
- [38] B. Doyon and T. Yoshimura, A note on generalized hydrodynamics: Inhomogeneous fields and other concepts, *SciPost Phys.* **2**, 014 (2017).
- [39] A. Bastianello, V. Alba, and J.-S. Caux, Generalized Hydrodynamics with Space-Time Inhomogeneous Interactions, *Phys. Rev. Lett.* **123**, 130602 (2019).
- [40] R. Dubessy, J. Polo, H. Perrin, A. Minguzzi, and M. Olshanii, Universal shock-wave propagation in one-dimensional Bose fluids, *Phys. Rev. Res.* **3**, 013098 (2021).
- [41] V. B. Bulchandani, R. Vasseur, C. Karrasch, and J. E. Moore, Bethe-Boltzmann hydrodynamics and spin transport in the XXZ chain, *Phys. Rev. B* **97**, 045407 (2018).
- [42] A. Urichuk, Y. Oez, A. Klümper, and J. Sirker, The spin Drude weight of the XXZ chain and generalized hydrodynamics, *SciPost Phys.* **6**, 005 (2019).
- [43] B. Doyon, H. Spohn, and T. Yoshimura, A geometric viewpoint on generalized hydrodynamics, *Nucl. Phys. B* **926**, 570 (2018).
- [44] S. A. Simmons, F. A. Bayocboc, J. C. Pillay, D. Colas, I. P. McCulloch, and K. V. Kheruntsyan, What is a Quantum Shock Wave? *Phys. Rev. Lett.* **125**, 180401 (2020).
- [45] K. F. Thomas, M. J. Davis, and K. V. Kheruntsyan, Thermalization of a quantum Newton's cradle in a one-dimensional quasicondensate, *Phys. Rev. A* **103**, 023315 (2021).
- [46] J.-S. Caux, B. Doyon, J. Dubail, R. Konik, and T. Yoshimura, Hydrodynamics of the interacting Bose gas in the Quantum Newton Cradle setup, *SciPost Phys.* **6**, 070 (2019).
- [47] J. D. Nardis, D. Bernard, and B. Doyon, Diffusion in generalized hydrodynamics and quasiparticle scattering, *SciPost Phys.* **6**, 049 (2019).
- [48] E. H. Lieb and W. Liniger, Exact analysis of an interacting Bose gas. I. The general solution and the ground state, *Phys. Rev.* **130**, 1605 (1963).
- [49] L. Pitaevskii and S. Stringari, *Bose-Einstein Condensation and Superfluidity*, International Series of Monographs on Physics, Vol. 164 (Oxford University, Oxford, 2016).
- [50] B. Damski, Formation of shock waves in a Bose-Einstein condensate, *Phys. Rev. A* **69**, 043610 (2004).
- [51] B. Damski, Shock waves in a one-dimensional Bose gas: From a Bose-Einstein condensate to a Tonks gas, *Phys. Rev. A* **73**, 043601 (2006).
- [52] K. V. Kheruntsyan, D. M. Gangardt, P. D. Drummond, and G. V. Shlyapnikov, Finite-temperature correlations and density profiles of an inhomogeneous interacting one-dimensional Bose gas, *Phys. Rev. A* **71**, 053615 (2005).
- [53] The condition for applicability of the SPGPE is  $|\mu| \ll k_B T$  [61], with the  $c$ -field region defined in terms of dimensionless interaction and temperature parameters by the condition  $\gamma \ll \bar{T} \ll 1$  [52,65], where the dimensionless temperature  $\bar{T}$  is defined according to  $\bar{T} = T/T_d$ , with  $T_d = \hbar^2 \rho_{\text{bg}}^2 / 2mk_B$  being the temperature of quantum degeneracy [52]. We further focus on the quasicondensate regime, which can be described by the Bogoliubov theory dominated by thermal (rather than vacuum) fluctuations, bounded by the condition  $\gamma \ll \bar{T} \ll \sqrt{\gamma}$  [65] (see also Refs. [87–89]). The truncated Wigner approximation, on the other hand, is valid when the total number of particles in the system  $N$  greatly exceeds the number of relevant Bogoliubov modes,  $M_B$  [62]. The systems investigated using this approach in Figs. 1(a)–1(c) were reported to follow this criterion in Ref. [44], where the ratio  $N/M_B$  was calculated to be  $N/M_B \approx 5$ , with variations around this value between  $N/M_B \approx 2$  and  $N/M_B \approx 10$  producing essentially the same results.
- [54] H. Spohn, *Large Scale Dynamics of Interacting Particles* (Springer, Berlin, 2012).
- [55] E. Bettelheim, The Whitham approach to the  $c \rightarrow 0$  limit of the Lieb–Liniger model and generalized hydrodynamics, *J. Phys. A: Math. Theor.* **53**, 205204 (2020).
- [56] G. B. Whitham, *Linear and Nonlinear Waves*, Pure and Applied Mathematics, Vol. 42 (Wiley & Sons, New York, 2011).
- [57] A. M. Kamchatnov, *Nonlinear Periodic Waves and Their Modulations: An Introductory Course* (World Scientific, Singapore, 2000).
- [58] C. Mora and Y. Castin, Extension of Bogoliubov theory to quasicondensates, *Phys. Rev. A* **67**, 053615 (2003).
- [59] M. A. Cazalilla, Bosonizing one-dimensional cold atomic gases, *J. Phys. B: At., Mol. Opt. Phys.* **37**, S1 (2004).
- [60] I. Bouchoule, M. Arzamasovs, K. V. Kheruntsyan, and D. M. Gangardt, Two-body momentum correlations in a weakly interacting one-dimensional Bose gas, *Phys. Rev. A* **86**, 033626 (2012).
- [61] Y. Castin, R. Dum, E. Mandonnet, A. Minguzzi, and I. Carusotto, Coherence properties of a continuous atom laser, *J. Mod. Opt.* **47**, 2671 (2000).
- [62] P. B. Blakie, A. Bradley, M. Davis, R. Ballagh, and C. Gardiner, Dynamics and statistical mechanics of ultra-cold Bose gases using  $c$ -field techniques, *Adv. Phys.* **57**, 363 (2008).
- [63] I. Bouchoule, S. S. Szigeti, M. J. Davis, and K. V. Kheruntsyan, Finite-temperature hydrodynamics for one-dimensional Bose gases: Breathing-mode oscillations as a case study, *Phys. Rev. A* **94**, 051602(R) (2016).
- [64] F. A. Bayocboc, M. J. Davis, and K. V. Kheruntsyan, Dynamics of thermalization of two tunnel-coupled one-dimensional quasicondensates, *Phys. Rev. A* **106**, 023320 (2022).
- [65] F. Bayocboc, Jr and K. Kheruntsyan, Frequency beating and damping of breathing oscillations of a harmonically trapped one-dimensional quasicondensate, *C. R. Phys.* **24**, 1 (2023).
- [66] For the examples considered in Fig. 1(d), the thermal phase coherence lengths are  $l_T/L \simeq 0.1$  for  $\bar{T} = 0.01$  and  $l_T/L \simeq 0.01$  for  $\bar{T} = 0.1$ . These values, in turn, are comparable or smaller than the width of the initial density bump  $\bar{\sigma} = 0.02$ , implying a reduced phase coherence over the extent of the bump and hence loss of interference contrast upon expansion of the bump into the background [44].
- [67] E. Bettelheim and L. Glazman, Quantum Ripples Over a Semi-classical Shock, *Phys. Rev. Lett.* **109**, 260602 (2012).
- [68] In the example of Fig. 1(e), which is for  $N = 1000$  particles, we have been able to discriminate between the Friedel oscillations,

which have a period of  $1/1000$ , and the Bettelheim-Glazman density ripples, which have a larger oscillation period. This was not possible in the prior work of Ref. [44], which treated a much smaller number of particles ( $N = 50$ ) in the Tonks-Girardeau regime.

- [69] M. Girardeau, Relationship between systems of impenetrable bosons and fermions in one dimension, *J. Math. Phys.* **1**, 516 (1960).
- [70] M. D. Girardeau and E. M. Wright, Dark Solitons in a One-Dimensional Condensate of Hard Core Bosons, *Phys. Rev. Lett.* **84**, 5691 (2000).
- [71] In the Tonks-Girardeau limit, there is an exact equivalence between GHD and the semiclassical Wigner function model of a free Fermi gas [14,67,90]. This model predicts a smooth density profile of the semiclassical shock, whereas quantum corrections, derived in Refs. [67,91,92], predict small-amplitude oscillations (“density ripples”) on top of the smooth density profile. These oscillations persist within a finite extent of the shock front for times well beyond shock formation [90] and have a frequency chirp that is in the opposite direction to the chirp of the interference fringes seen in GPE simulations of dispersive shock waves in the weakly interacting regime.
- [72] J. J. Chang, P. Engels, and M. A. Hoefer, Formation of Dispersive Shock Waves by Merging and Splitting Bose-Einstein Condensates, *Phys. Rev. Lett.* **101**, 170404 (2008).
- [73] F. S. Møller and J. Schmiedmayer, Introducing iFluid: A numerical framework for solving hydrodynamical equations in integrable models, *SciPost Phys.* **8**, 041 (2020).
- [74] See Supplemental Material at <http://link.aps.org/supplemental/10.1103/PhysRevResearch.5.L022024>, which outlines the theory of generalized hydrodynamics for the one-dimensional Bose gas at Euler and Navier-Stokes scales, along with the presentation of further analysis of the quantum Newton’s cradle, including the case of a Bragg pulse protocol [1,45,93,94] and a comparison of evolving and relaxed density profiles in terms of the Bhattacharyya distance [95].
- [75] C. N. Yang and C. P. Yang, Thermodynamics of a one-dimensional system of bosons with repulsive Delta-function interaction, *J. Math. Phys.* **10**, 1115 (1969).
- [76] A. H. van Amerongen, J. J. P. van Es, P. Wicke, K. V. Kheruntsyan, and N. J. van Druten, Yang-Yang Thermodynamics on an Atom Chip, *Phys. Rev. Lett.* **100**, 090402 (2008).
- [77] M. J. Davis, P. B. Blakie, A. H. van Amerongen, N. J. van Druten, and K. V. Kheruntsyan, Yang-Yang thermometry and momentum distribution of a trapped one-dimensional Bose gas, *Phys. Rev. A* **85**, 031604 (2012).
- [78] J. Mossel and J.-S. Caux, Generalized TBA and generalized Gibbs, *J. Phys. A: Math. Theor.* **45**, 255001 (2012).
- [79] It was argued recently in Ref. [19] that the stationary states within fluid cells are attained entirely in the time window where diffusive dynamics are the dominant contribution beyond the Euler scale and that these stationary states are uniquely described by the thermal ensemble. Following this window, higher-order corrections beyond diffusion must be incorporated, however, as thermal states are stationary under exact evolution via the Lieb-Liniger Hamiltonian, the relaxed state will remain thermal beyond this window.
- [80] J. Armijo, T. Jacqmin, K. V. Kheruntsyan, and I. Bouchoule, Probing Three-Body Correlations in a Quantum Gas Using the Measurement of the Third Moment of Density Fluctuations, *Phys. Rev. Lett.* **105**, 230402 (2010).
- [81] M. Olshanii, Atomic Scattering in the Presence of an External Confinement and a Gas of Impenetrable Bosons, *Phys. Rev. Lett.* **81**, 938 (1998).
- [82] G. El and M. Hoefer, Dispersive shock waves and modulation theory, *Phys. D (Amsterdam, Neth.)* **333**, 11 (2016).
- [83] A. V. Gurevich and L. P. Pitaevskii, Nonstationary structure of a collisionless shock wave, *Zh. Eksp. Teor. Fiz.* **65**, 590 (1973).
- [84] J. Dziarmaga, Z. P. Karkuszewski, and K. Sacha, Images of the dark soliton in a depleted condensate, *J. Phys. B: At., Mol. Opt. Phys.* **36**, 1217 (2003).
- [85] J. Dziarmaga, Quantum dark soliton: Nonperturbative diffusion of phase and position, *Phys. Rev. A* **70**, 063616 (2004).
- [86] A. D. Martin and J. Ruostekoski, Quantum and Thermal Effects of Dark Solitons in a One-Dimensional Bose Gas, *Phys. Rev. Lett.* **104**, 194102 (2010).
- [87] J. Pietraszewicz and P. Deuar, Classical field records of a quantum system: Their internal consistency and accuracy, *Phys. Rev. A* **92**, 063620 (2015).
- [88] J. Pietraszewicz and P. Deuar, Classical fields in the one-dimensional Bose gas: Applicability and determination of the optimal cutoff, *Phys. Rev. A* **98**, 023622 (2018).
- [89] J. Pietraszewicz and P. Deuar, Complex wave fields in the interacting one-dimensional Bose gas, *Phys. Rev. A* **97**, 053607 (2018).
- [90] T. Veness and L. I. Glazman, Fate of quantum shock waves at late times, *Phys. Rev. B* **100**, 235125 (2019).
- [91] E. Bettelheim and P. B. Wiegmann, Universal Fermi distribution of semiclassical nonequilibrium Fermi states, *Phys. Rev. B* **84**, 085102 (2011).
- [92] I. V. Protopopov, D. B. Gutman, P. Schmitteckert, and A. D. Mirlin, Dynamics of waves in one-dimensional electron systems: Density oscillations driven by population inversion, *Phys. Rev. B* **87**, 045112 (2013).
- [93] S. Wu, Y.-J. Wang, Q. Diot, and M. Prentiss, Splitting matter waves using an optimized standing-wave light-pulse sequence, *Phys. Rev. A* **71**, 043602 (2005).
- [94] Y. Y. Atas, D. M. Gangardt, I. Bouchoule, and K. V. Kheruntsyan, Exact nonequilibrium dynamics of finite-temperature Tonks-Girardeau gases, *Phys. Rev. A* **95**, 043622 (2017).
- [95] A. Bhattacharyya, On a measure of divergence between two statistical populations defined by their probability distributions, *Bull. Calcutta Math. Soc.* **35**, 99 (1943).